Geophysical Research Letters

RESEARCH LETTER
10.1029/2021GL094581

Key Points:

- Long-term monitoring of daytime very low frequency (VLF) amplitudes shows a spring-fall asymmetry with unexpected enhancements during fall
- Mean annual temperature at 70–80 km, with removed symmetric level, shows a deviation during fall that anticorrelates with the VLF behavior
- The semidiurnal solar tide amplitude at 70–80 km is also enhanced during fall, suggesting the influence of a mean zonal wind reversal

Supporting Information:

Supporting Information may be found in the online version of this article.

Correspondence to:

E. L. Macotela,
edithlilianamc@gmail.com

Citation:

Macotela, E. L., Clilverd, M., Renkwitz, T., Chau, J., Manninen, J., & Banyś, D. (2021). Spring-fall asymmetry in VLF amplitudes recorded in the North Atlantic region: The fall-effect. *Geophysical Research Letters*, *48*, e2021GL094581. https://doi.org/10.1029/2021GL094581

Received 2 JUN 2021
Accepted 23 JUL 2021

Spring-Fall Asymmetry in VLF Amplitudes Recorded in the North Atlantic Region: The Fall-Effect

E. L. Macotela[1,2], M. Clilverd[3], T. Renkwitz[2], J. Chau[2], J. Manninen[4], and D. Banyś[5]

[1]Faculty of Mathematics and Natural Sciences, University of Rostock, Rostock, Germany, [2]Leibniz-Institute of Atmospheric Physics, University of Rostock, Kuehlungsborn, Germany, [3]British Antarctic Survey, UKRI-NERC, Cambridge, UK, [4]Sodanklä Geophysical Observatory, University of Oulu, Sodankyla, Finland, [5]Institute for Solar-Terrestrial Physics, German Aerospace Center, Neustrelitz, Germany

Abstract A spring-fall asymmetry is observed in daytime amplitude values of very low frequency (VLF) radio wave signals propagating over the North Atlantic during 2011–2019. We explore the processes behind this asymmetry by comparing against mesospheric mean temperatures and the semidiurnal solar tide (S2) in mesospheric winds. The solar radiation influence on VLF subionospheric propagation was removed from the daytime VLF amplitude values, isolating the fall-effect. Similarly, the symmetric background level was removed from mesospheric mean temperatures undertaking comparable analysis. During fall, all three analyzed parameters experience significant deviation from their background levels. The VLF amplitude variation during spring is explained by the seasonal variation in solar illumination conditions, while the fall-effect can be interpreted as a mean zonal wind reversal associated with both a S2 enhancement, and temperature reductions. Decreases in temperature can produce decreases in collision frequency, reducing VLF signal absorption, driving the observed VLF asymmetry.

Plain Language Summary The ionosphere is useful for it makes long-distance radio communication possible. Its lower boundary is called the D-region (60–90 km) and can be monitored using the very low frequency technique, VLF for short. VLF radio signals propagate long distances in the Earth-ionosphere waveguide. Monitoring the annual variability of the signal's amplitude measured in Northern Finland during daytime, a comparative amplitude asymmetry during spring and fall seasons is observed, for which the responsible mechanism is still unknown. Here, we report a multiyear analysis of this asymmetry observed using VLF signals propagating at middle-to-high latitudes. Around the D-region altitudes, the sun induces oscillations in the wind dynamics called solar tides. At the same altitudes, the mesospheric mean temperature has the unique characteristic of a cool summer and a warm winter. We put forward the hypothesis that, during fall, the mean zonal wind reverses from westerly to easterly, and this is associated with both semidiurnal solar tide enhancement, and mean temperature changes. The latter can affect the chemistry and dynamics in the D-region in a significant way, eventually changing the VLF propagation condition, and therefore, the amplitude strength.

1. Introduction

Very low frequency (VLF: 3–30 kHz) radio waves propagate inside the Earth-ionosphere waveguide monitoring the electrical conductivity of its boundaries. The upper boundary properties of the waveguide can be represented by Wait parameters (Wait & Spies, 1964), namely, the reference height and conductivity gradient of the D-region. The quiescent ionospheric condition can be disturbed by different types of physical phenomena, originating in space (Clilverd et al., 2010; Macotela et al., 2017) or on Earth (Macotela, Clilverd, Manninen, Thomson, et al., 2019). These disturbances, interpreted as perturbations of the D-region ionization levels, produce changes in the Wait parameters, which show up as phase and/or amplitude variations in the VLF signals.

It is well known that the long-term variation of the daytime lower ionosphere exhibits distinct seasonal characteristics with high variability in winter, and lower variability in summer (Bertoni et al., 2013; Correia et al., 2011; Macotela, Clilverd, Manninen, Moffat-Griffin, et al., 2019). The D-region, created and maintained by solar radiation (Nicolet & Aikin, 1960), depends on the solar zenith angle (SZA), which is a func-

tion of time of day, date, and latitude on Earth. This function is symmetric with respect to the maximum of illumination. Thus, the seasonal VLF amplitude is expected to follow the SZA variation. However, here we report cases where this expected variation is not followed.

Analysis of long-term VLF amplitude signal propagating in the northern hemisphere showed a comparative asymmetry during spring and fall seasons (Macotela, Clilverd, Manninen, Moffat-Griffin, et al., 2019) but was not investigated at the time. Recently, reviewing the data once more, we realized that this observation has not been sufficiently studied and the mechanism that generates this asymmetry is yet unknown. A few studies have previously reported a seasonal asymmetry in the VLF attenuation data (Greninger, 2016; Korsakov, et al., 2020). Korsakov et al. (2020) explained their findings considering the sensitivity of vertical antennas to environmental factors such as temperature and humidity. In contrast, the VLF measurements analyzed in this study are obtained from loops antennas, which are largely insensitive to such environmental factors (Watt, 1967).

Here, we present a multiyear analysis of the spring-fall asymmetry observed in the amplitude of VLF signals propagating over the North Atlantic and recorded between 2011 and 2019. Thus, in this manuscript the terms indicating the seasons correspond to the northern hemisphere. We show that the amplitude values during fall are enhanced above those seen during equivalent SZA conditions in spring, and so for brevity we use the term fall-effect.

2. The Spring-Fall Asymmetry

2.1. Observation in VLF Data

In this study, narrow band subionospheric VLF amplitude data were analyzed from the 19.58 kHz (UK), 37.5 kHz (Iceland) and 24.0 kHz (USA) transmitters, recorded at either Sodankylä (SOD) or Kilpisjärvi (KIL), Finland. The transmitters' call signs are GQD, NRK, and NAA, respectively. From these transmitter and receiver combinations there is data continuity for four propagation paths, which are: NRK-KIL, GQD-KIL, NRK-SOD, and NAA-SOD. The spatial configurations of the sites, together with the propagation paths, are shown in Figure S1. This configuration allows us to analyze signals propagating between middle- and high-latitudes. The length of the propagation paths and the localization of the transmitters and receivers are described in Table S1.

The receivers are part of the Antarctic-Arctic Radiation-belt (Dynamic) Deposition–VLF Atmospheric Research Konsortium (AARDDVARK) network (Clilverd et al., 2009) which provides continuous long-range observations of the lower ionosphere, particularly in the Polar Regions. The receivers are composed of two orthogonally oriented magnetic field loop antennas, and the recording system uses the UltraMSK software, which measures both the phase and amplitude of Minimum Shift Keying modulated narrowband VLF radio signals (Clilverd et al., 2009). Furthermore, the receivers include an effective impulsive sferic noise suppression.

The seasonal variation of the daytime VLF amplitudes was computed using two-hour average around the time of maximum solar illumination. For NAA-SOD this time changes throughout the year in about 40 min, with its average at 14:41 UTC. This approach minimizes the impact of any ionospheric short-term fluctuations as well as any effect due to the time shift of the maximum solar illumination. The measurements during NAA maintenance days were automatically considered as missing data, with a lower threshold of −90 dB during winter and −73 dB during summer.

Figure 1 shows the step-by-step analysis for one VLF path, NAA-SOD. The evolution of these daily averages as a function of the day of year, from 2011 until 2019, differentiated by the colored lines, is shown in Figure 1a. As expected, a large (smooth) variability is observed in winter (summer). When comparing spring and fall, a clear asymmetry is noted. During spring, the amplitude increases slowly. Whereas, during fall the amplitude is initially high, followed by a sudden and fast decrease of its strength in early October.

Figure 1b shows in dashed line the average of the amplitudes displayed in the top panel smoothed using a 21-day time window (to compare it with the tidal analysis, Section 2.3) as well as its standard deviation of $\pm 0.5\sigma$ (dotted lines). Here, the spring-fall asymmetry is more evident. The daytime D-region ionization depends on the solar illumination conditions, which is inferred from the SZA. Thus, the average SZA

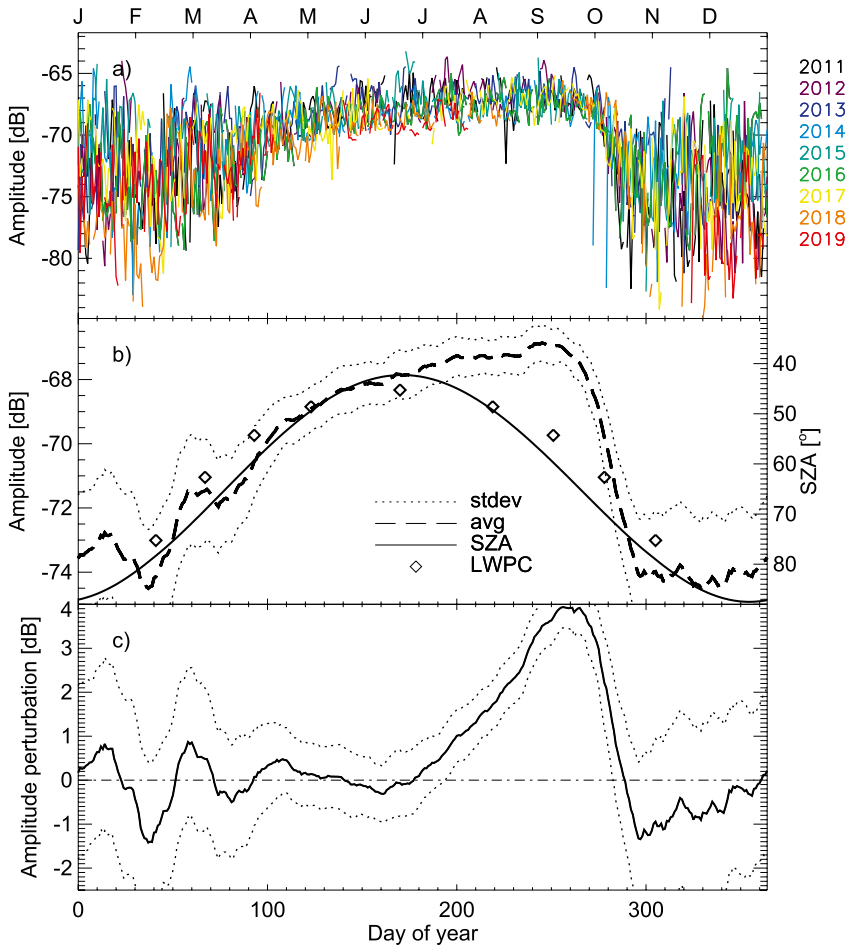

Figure 1. (a) Temporal variation of 2-h around the maximum solar illumination for years 2011–2019, differentiated by colored lines as indicated in the legend, for NAA-SOD. (b) Climatological average of the curves in (a) smoothed using a 21-day time window (dashed line). The dotted curves are ±0.5σ computed in dB. The solid curve is the temporal evolution of the average solar zenith angle (SZA) for the propagation path. The diamonds are the long wave propagation code (LWPC)-amplitude obtained for specific SZA at 79°, 70°, 60°, 50°, and 43°. (c) Amplitude perturbation after removing its corresponding SZA-driven amplitude. Dotted lines are ±0.5σ and the dot-dashed line represents zero amplitude.

computed at 50 equidistant points along the propagation path at the time of the maximum illumination is employed. Figure 1b displays the time evolution of this average SZA through the year (thin continuous line). In this figure, the VLF amplitude behavior between mid-summer to fall (days 191–283) exhibits a significant deviation from the expected values.

To confirm this, the equivalent VLF amplitude was calculated using the Long Wave Propagation Code (LWPC, Ferguson, 1998), which makes it possible to determine VLF signal strength as a function of distance. The LWPC amplitude was computed for five fixed SZA values, 79°, 70°, 60°, 50°, and 43°, assuming constant values of Wait parameters along the propagation path and employing the McRae and Thomson (2000) and Thomson et al. (2017) SZA relationships. These authors reported the SZA and Wait parameters relationship for different regions on Earth and for different levels of a 11-year solar activity cycle. Therefore, employing their average provides a better representation of the D-region variation on the various paths studied here, over long time periods. The LWPC amplitude is shown in Figure 1b (diamonds), confirming that the expected temporal evolution of the quiet daytime ionosphere follows the SZA variation.

A quadratic fit between the SZA and the average VLF amplitude from day 1 to mid-summer (day 180) was used to compute the SZA-driven amplitude. Figure 1c shows the subtraction of both amplitudes (solid) together with its ±0.5σ (dotted). The horizontal dot-dashed line indicates the zero level. Considering the

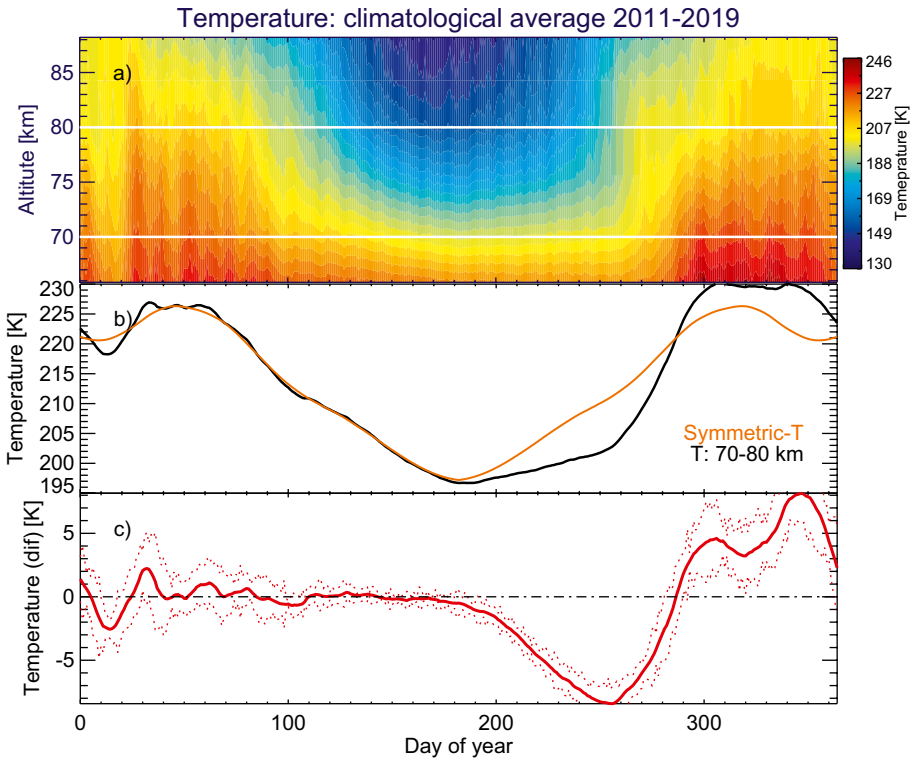

Figure 2. (a) Vertical overview of the climatological average of Microwave Limb Sounder (MLS) atmospheric temperature since 2011 until 2019, for the geographic region around the very low frequency (VLF) propagation paths. The horizontal white lines delimit the 70–80 km altitude range. (b) Time evolution of the MLS average temperature at this altitude (black), and its symmetric background level (orange). (c) The difference between the MLS temperature at 70–80 km and its symmetric background level. The dot-dashed line represents the zero level, and the dotted curves are $\pm 0.5\sigma$.

standard deviation, a departure in the signal from the zero level is observed from day 191 to day 283, lasting about 3 months, with a slow increase and a fast recovery. The maximum value of the deviation is ∼4 dB, and it occurs around day 264.

The same procedure is applied to the other three VLF data sets and the results are found to be similar, as observed in Figures S2, S3, and S4. We describe the enhancement anomaly occurring in the fall season as the *fall-effect* throughout the rest of this study.

2.2. Observation in Mesospheric Temperatures

The Earth Observing System Microwave Limb Sounder (MLS) onboard the Aura spacecraft measures thermal emission from the Earth's atmosphere (Waters et al., 2006). Aura coverage is from 82°S to 80°N, with ∼13 orbits per day, and limb scanning from close to the ground up to ∼100 km. The MLS instrument provides daily global measurements of temperature and chemical constituents vertical profiles (Waters et al., 2006). The MLS v5.0x level 2 temperature data was screened using Livesey et al. (2020) quality control criteria, such as, using the recommended vertical pressure range for scientific use, 261–0.00046 hPa. For the analysis, three areas that enclose the four VLF propagation paths wewe chosen. These areas are: (i) 44°N–68°N, 70°W–30°W; (ii) 60°N–71°N, 30°W–30°E; and (iii) 53°N–60°N, 4°W–4°E; and are shown as boxes in Figure S1.

An overview of the climatological average of the MLS atmospheric temperature data set, for years 2011–2019, for the altitude range 65–95 km is shown in Figure 2a. Here, a clear seasonal variation is observed. Interestingly, the measurements in spring and fall also follow an asymmetric behavior, with a slower rate of change in temperature from summer to mid fall when compared to the one from spring to summer. This be-

havior in the mean temperature agrees with previous reports (Herron, 2004; Lübken, 1999). The horizontal white lines delimit the altitude range between 70 and 80 km that is analyzed further. This range was selected because during daytime the VLF waves reflect at these altitudes, and it is also in agreement with the reference height variation of McRae and Thomson (2000) and Thomson et al. (2017), employed in the LWPC computation. The black curve in Figure 2b shows the average temperature at 70–80 km smoothed using a 21-day time window length. The orange curve shows the symmetric background level computed using the first half of the average temperature (black) with a 31-day smoothing. This one-month time window moving average was chosen to identify the seasonal variation of the background temperature. From these two temperatures, a clear difference is observed from mid-summer to fall. This difference and its $\pm 0.5\sigma$ are shown in Figure 2c. Comparing this temperature perturbation behavior with that of the VLF perturbation (Figure 1c), a remarkable similarity is observed. A clear deviation is noted in the temperature difference around fall, reaching a minimum value during mid-fall.

2.3. Observations in Mesospheric Winds and the Semidiurnal Solar Tide

Zonal and meridional wind data from the Saura medium frequency radar, (69.14°N; 16.02°E; Renkwitz et al., 2018; and Singer et al., 2008), was used in this study. Specifically, data from 2011 to 2019 for the altitude range 60–95 km, time resolution of 1 h, and altitude resolution of 1 km. From these horizontal winds, the semidiurnal atmospheric solar tide (S2) was derived. Tides are global-scale oscillations in wind (or temperature, density, etc.) at periods which are subharmonics of a solar day. In this study, we assume that tides result from a linear superposition of a mean background flow and different period waves (e.g., Chau et al., 2015; Stening et al., 1997). Thus, the following equation can be independently fit to the zonal and meridional winds (e.g., Sandford et al., 2006):

$$\left(u,v\right) = \left(u_0,v_0\right) + \sum_{i=1}^{n}\left(a_u,a_v\right)\cos\left(2\pi\frac{t}{T_i}\right) + \left(b_u,b_v\right)\sin\left(2\pi\frac{t}{T_i}\right) \quad (1)$$

where, u and v are the estimated zonal and meridional winds; u_0 and v_0 are the mean zonal and meridional wind; a_u, a_v, b_u, b_v are the coefficients of the wave amplitudes for each wind component; t is the time in hours; and T is the period of each considered wave ($T_1 = 12$ h). Equation 1 was solved using the least-square method with a running window of 21 days. This window was applied in order to compare the results with previous reports.

Figure 3a displays the climatological average of the time-altitude variation of u_0. The figure shows that u_0 is eastward during winter and westward during summer. The wind reversals are indicated by the black lines, and they occur during mid spring and fall. The black box in the lower right corner indicates unreliable data. Figure 3b illustrates the climatological average of the total magnitude of S2 tide ($\sqrt{a_u^2 + b_u^2 + a_v^2 + b_v^2}$), using both wind components, u and v, as a function of altitude and time. Again, the black box indicates unreliable data. Figure 3b shows that S2 increases with the altitude, especially during winter and mid fall, in agreement with previous findings for middle- and high-latitudes (Conte et al., 2018; He & Chau, 2019; Laskar et al., 2016). Similarly, as in the case of temperature and VLF parameters, an asymmetric behavior of S2 is also observed, with larger amplitudes during fall but not during spring. In addition, between 70 and 80 km, indicated by horizontal white lines, there is a single enhancement in the tide amplitude characterized by a downward transport of S2, from day 230 to a sudden depletion around day 280. The temporal variation of the average S2 tide for this altitude range is shown in Figure 3c. From this curve, a well-defined enhancement is observed for S2 amplitudes, with a peak well above 12 m/s. As in the case of the temperature analysis, the S2 enhancement matches in time and shape with the VLF perturbation, with a maximum occurring just after the time of the mean zonal wind reversal.

Figure 4a shows the fall-effect observed in the amplitude of VLF data for the four propagation paths, which are differentiated by colored lines. We provide its average value (black) and the zero level (dashed) in Figure 4b to simplify comparisons with the other parameters. This average can be considered as the representative VLF amplitude fall-effect perturbation over the North Atlantic. Figure 4b also shows the fall-effect observed in mesospheric temperature (red) and S2 solar tide (cyan) that were shown in Figures 2c and 3b, respectively, yet are displayed here for comparison. Linear correlation coefficients of the VLF perturbation with MLS temperature, also and S2 tide, were computed between 65 and 95 km for every 10 km. As expect-

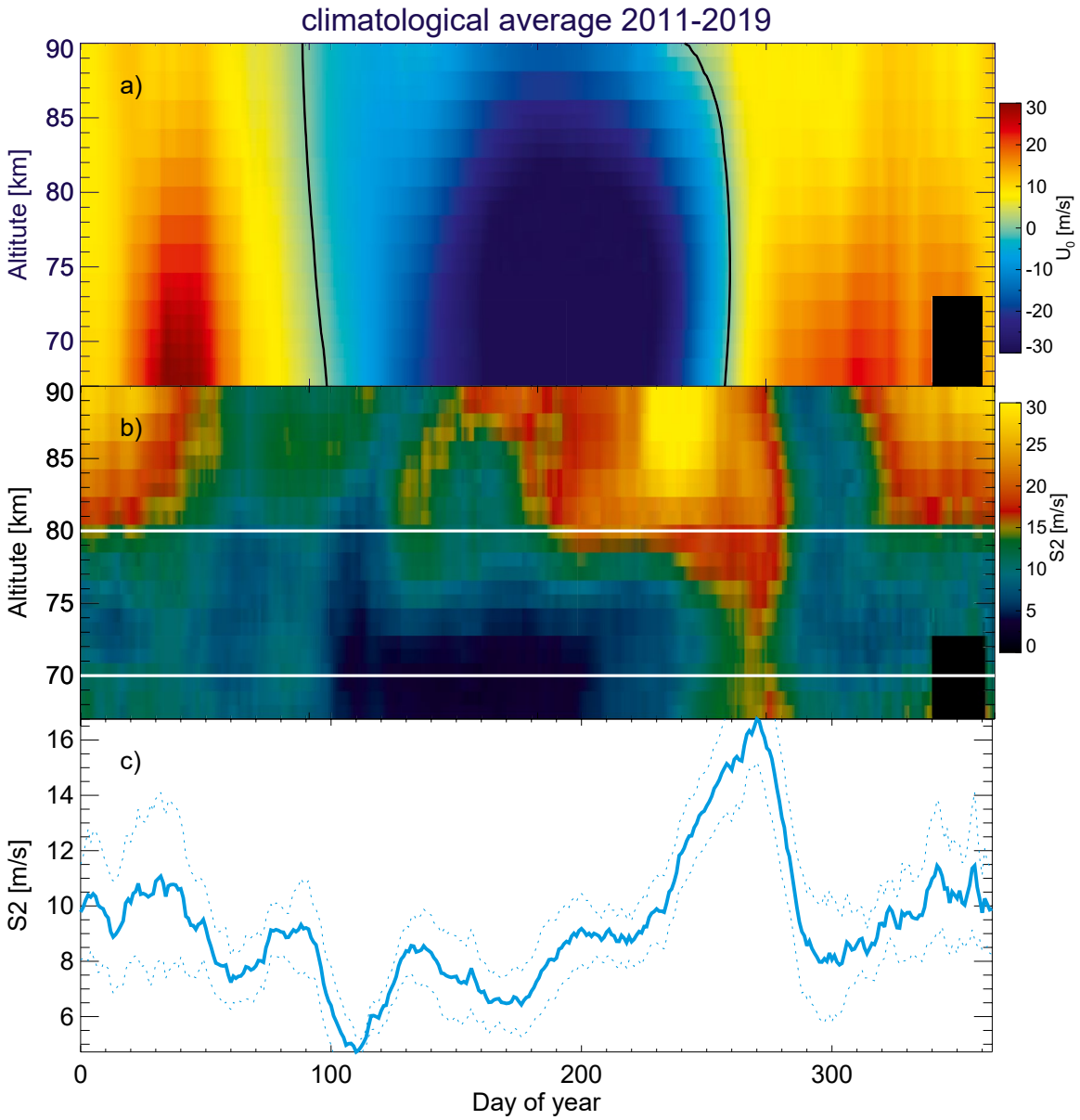

Figure 3. Annual climatological average (2011–2019) as a function of altitude of (a) u_0 and (b) S2 solar tide over Norway. The black curve represents zero speed indicating wind reversal. The horizontal white lines delimit the altitude range 70–80 km. (c) The temporal evolution of S2 tide for 70–80 km altitude range (solid) and its ±0.5σ represented by dotted curves.

ed, the correlation is highest for the altitude range 70–80 km used to compute the average curves shown here. Figure 4b shows that during fall, a negative temperature deviation occurs while the VLF amplitude increases. It is also observed that temperature and VLF variations closely follow each other throughout the year. In addition, a high negative correlation of $R_{\text{T-VLF}} = 0.82$ is found between these two parameters, with high significance. Contrary to the temperature analysis, an out of phase behavior between the S2 tide and VLF variability parameters is perceived during other periods of the year, despite being in phase during the fall-effect period. However, their linear correlation coefficient ($R_{\text{S2-VLF}} = 0.67$) is still high. Furthermore, we note that the S2 tide starts its fall-effect about 20 days later than the corresponding effect in temperature or VLF amplitude perturbations.

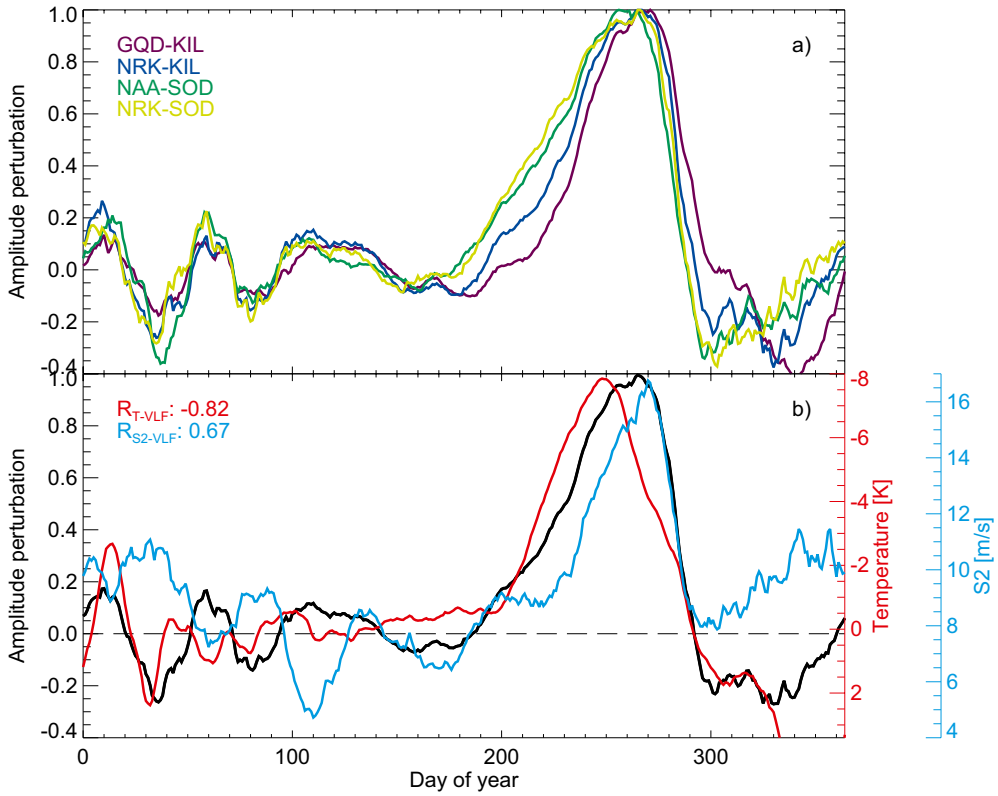

Figure 4. a) The obtained very low frequency (VLF) amplitude perturbation for the four propagation paths indicated by the colored lines. (b) The average VLF amplitude perturbation over the North Atlantic (black), mesospheric temperature (red), and S2 tide (cyan). The correlation coefficients of temperature–amplitude perturbation ($R_{T\text{-}VLF}$) and S2–amplitude perturbation ($R_{S2\text{-}VLF}$) is indicated in the legend.

3. Discussion and Concluding Remarks

VLF measurements recorded in Northern Finland from 2011 to 2019 have been used to identify a spring-fall asymmetry in the daily daytime VLF amplitude values. This asymmetry is observed in signals propagating on four different VLF paths.

Daytime VLF amplitudes during spring follow the solar illumination variation, while those during fall do not. Indeed, this associated temporal evolution for most of the year justifies the removal of the SZA-driven background level in the VLF data series. The effect observed during fall was isolated and analyzed to understand its most plausible generation mechanism. D-region forcing factors originating from space are less likely to be responsible since those phenomena have shorter (e.g., gamma ray bursts) or longer (e.g., solar cycle) time scales than the observed fall-effect. Thus, changes in the Earth's atmosphere seems the most plausible source.

Watt (1967) showed the seasonal variation of attenuation rates for VLF waves without any spring-fall asymmetry. This is not a surprise since the theory of VLF propagation, widely used, is based on a simple exponential model for the reflecting base of the ionosphere and does not consider the influence of atmospheric wave's dynamics. Thus, Figure 1b confirms that the simple SZA-based model employed so far is not always an effective way of reproducing the actual D-region properties.

To explain our climatological observations, we put forward the following hypothesis: stratospheric mean zonal wind reversal can be associated with both S2 enhancements and temperature changes. These changes in temperature ultimately affect the VLF amplitude strength (i.e., wind reversal→S2; and wind reversal→T→VLF). From the observations (Figure 3a), reversal of the mean zonal wind velocity, from westerly to easterly, occurs during the fall equinox. The weak velocity (nearly zero) has a high impact on atmospheric wave propagation conditions, leading to enhancements in tidal variability and gravity-wave transmission

from the lower atmosphere (Conte et al., 2018; Espy & Stegman, 2002; Laskar et al., 2016). Even though the wind reversal time in Figure 3a corresponds to mesospheric altitudes, it is reasonable to expect it to occur some days earlier than at stratospheric altitudes. This is confirmed in Figure 9 of Pedatella et al. (2021), who analyzed Specified Dynamics Whole Atmosphere Community Climate Model with thermosphere-ionosphere eXtension (SD-WACCMX) simulations. In addition, Conte et al. (2018) reported that meteor radar observations show an increase in gravity wave activity during the fall equinox. This suggests that the increase in the amplitude of S2 tide may be partly due to its interaction with gravity waves as a result of the reversal of the mean zonal wind. The ∼20-day delay in the start of the fall-effect for S2 when compare to the temperature or VLF amplitude perturbations, is not fully understood at present. However, we note out that S2 is obtained from single point measurements rather than over the large area where VLF and MLS analysis is undertaken, and this may contribute to the differences observed.

The role of gravity wave propagation and dissipation has been accepted as the dominant wave forcing that drives the circulation in the mesosphere lower thermosphere region (Smith, 2012), which is responsible for the cold summer mesopause. The seasonal variation of magnitude and pattern of mesospheric temperature has been examined at middle- and high-latitudes (Lübken, 1999; Shepherd et al., 2004; Singer et al., 2003). Such examinations showed a sharp decrease in temperature from spring to summer and a moderate increase from summer to fall, observed at middle-latitudes and up to ∼65°N. However, no explanation on this behavior has been reported. Lübken (1999) ruled out any systematic effect and also a tidal modulation from the observation. On the other hand, Singer et al. (2003) suggested that tides may influence this behavior. These studies lead us to suggest that the observed variation in temperature during fall may be caused by the interaction of the background wind and waves, such as gravity waves and planetary waves, which shall be addressed in detail in a follow-up study.

To describe the VLF and temperature relationship, we consider modifications in the lower ionospheric properties, which are sensed by the propagation of subionospheric VLF waves. Since the D-region mean free path is sufficiently short, we assume that ion, electron, and neutral temperatures are equal during undisturbed conditions (Enell et al., 2005). We also consider that the lower boundary of the ionosphere is not a mirror-type surface. In other words, VLF waves penetrate into the D-region up to the altitude where the wave frequency matches the plasma frequency of the medium. While propagating inside the D-region the VLF wave suffers deviative absorption (Hunsucker & Hargreaves, 2003). This type of absorption occurs near the level of reflection. In this case, the wave energy is dissipated in proportion to the collision frequency, ν. Under this condition, the absorption may actually decrease as ν diminishes, which is temperature dependent (Chilton, 1981). Thus, a decrease in temperature implies a deviative absorption reduction. This is observed in the VLF signal as an increase of VLF amplitude, corresponding to the results of the present study. The fact that the VLF variability follows the temperature variability throughout the year confirms that these two parameters are closely related. This relationship has also been pointed out previously by Silber et al. (2013). The short and weak fluctuations in the temperature and VLF variability, with positive or negative time lags between them, can be disregarded because they are within the error bars of the measurements.

Certainly, more data is required to be able to confirm whether the fall effect is related to the seasonal transition of the mean zonal wind impact on mean temperature, and whether the effect is also observed in other regions of the Earth or not. In the literature, we found a few graphs suggesting the presence of the fall-effect in VLF data (Clilverd et al., 2010; Correia et al., 2011; Macotela, Clilverd, Manninen, Moffat-Griffin, et al., 2019; Neal et al., 2015; Pal & Hobara, 2016). But the investigation of such effects was not the focus of those studies. All those studies used similar approaches to ours to monitor the daily amplitude variation during daytime, that is, averaging a few hours of the daytime VLF amplitude. Yet, those observations were made at different places, during different periods of time, and with different instrumentation than ours. Furthermore, there have been a few suggestions of an electron density profile sharp transition during fall for the lower ionosphere (Al'pert Ya, 1972; Pancheva & Mukhtarov, 1996). This could imply that the phenomena we observe may not be uncommon after all.

Finally, we consider that the observations presented in this letter and their particular characteristics open interesting research possibilities in understanding processes and dynamics of the lower ionosphere and mesosphere. Thus, more observational data from various resources, in the topic addressed here, needs to be

investigated and reported, especially if they were obtained at different geographical locations, and during different periods of the solar cycle activity.

Data Availability Statement

Data supporting this study are available via: http://doi.org/10.5281/zenodo.4883021 (VLF); https://acdisc.gesdisc.eosdis.nasa.gov/data/Aura_MLS_Level2/ML2T.005/ (MLS); https://www.radar-service.eu/radar/en/dataset/QHfWHaEtVYmUoqxq?token=HViGEGXykFmuMikBEWPn (MFR).

Acknowledgments
This work is supported by "AMELIE - Analysis of the MEsosphere and Lower Ionosphere fall Effect" (DLR project D/921/67286532). The authors thank Alexander Kozlovsky for providing his insights for this research work, in particular for looking mesospheric temperature data. MAC would like to acknowledge support from the UK Research and Innovation (UKRI-NERC) through National Capability Space Weather Observatory funding (NC-SS SWO). Open access funding enabled and organized by Projekt DEAL.

References

Al'pert Ya, L. (1972). *Propagation of electromagnetic waves in the ionosphere* (p. 564). Moscow. Nauka.

Bertoni, F. C. P., Raulin, J. -P., Gavilán, H. R., Kaufmann, P., Rodriguez, R., Clilverd, M., et al. (2013). Lower ionosphere monitoring by the South America VLF Network (SAVNET): C region occurrence and atmospheric temperature variability. *Journal of Geophysical Research: Space Physics*, *118*, 6686–6693. https://doi.org/10.1002/jgra.50559

Chau, J. L., Hoffmann, P., Pedatella, N. M., Matthias, V., & Stober, G. (2015). Upper mesospheric lunar tides over middle and high latitudes during sudden stratospheric warming events. *Journal of Geophysical Research: Space Physics*, *120*, 3084–3096. https://doi.org/10.1002/2015JA020998

Chilton, C. J. (1981). *Wave interaction observations of ionospheric modification in the D-region*. U.S. Department of Commerce, National Telecommunications and Information Administration.

Clilverd, M. A., Rodger, C. J., Gamble, R. J., Ulich, T., Raita, T., Seppälä, A., et al. (2010). Ground-based estimates of outer radiation belt energetic electron precipitation fluxes into the atmosphere. *Journal of Geophysical Research*, *115*, A12304. https://doi.org/10.1029/2010JA015638

Clilverd, M. A., Rodger, C. J., Thomson, N. R., Brundell, J. B., Ulich, T., Lichtenberger, J., et al. (2009). Remote sensing space weather events: Antarctic-Arctic radiation-belt (dynamic) deposition-VLF atmospheric research Konsortium network. *Space Weather*, *7*, S04001. https://doi.org/10.1029/2008SW000412

Conte, J. F., Chau, J. L., Laskar, F. I., Stober, G., Schmidt, H., & Brown, P. (2018). Semidiurnal solar tide differences between fall and spring transition times in the Northern Hemisphere. *Annales Geophysicae*, *36*, 999–1008. https://doi.org/10.5194/angeo-36-999-2018

Correia, E., Kaufmann, P., Raulin, J.-P., Bertoni, F., & Gavilan, H. R. (2011). Analysis of daytime ionosphere behavior between 2004 and 2008 in Antarctica. *Journal of Atmospheric and Solar-Terrestrial Physics*, *73*(16), 2272–2278. https://doi.org/10.1016/j.jastp.2011.06.008

Enell, C.-F., Kero, A., Turunen, E., Ulich, T., Verronen, P. T., Seppälä, A., et al. (2005). Effects of D-region RF heating studied with the Sodankylä Ion Chemistry model. *Annales Geophysicae*, *23*, 1575–1583. https://doi.org/10.5194/angeo-23-1575-2005

Espy, P. J., & Stegman, J. (2002). Trends and variability of mesospheric temperature at high-latitudes. *Physics and Chemistry of the Earth, Parts A/B/C*, *27*(6–8), 543–553. https://doi.org/10.1016/S1474-7065(02)00036-0

Ferguson, J. A. (1998). *Computer programmes for assessment of long wavelength radio communications, version 2.0, Tech. doc. 3030*. San Diego, California. Space and Naval Warfare Syst. Cent.

Greninger, P. (2016). *Seasonality of VLF attenuation through the ionosphere (Doctoral dissertation)*. University of New Mexico. Retrieved from https://digitalrepository.unm.edu/phyc_etds/18

He, M., & Chau, J. L. (2019). Mesospheric semidiurnal tides and near-12 h waves through jointly analyzing observations of five specular meteor radars from three longitudinal sectors at boreal midlatitudes. *Atmospheric Chemistry and Physics*, *19*, 5993–6006. https://doi.org/10.5194/acp-19-5993-2019

Herron, J. (2004). *Mesospheric temperature climatology above Utah state university (doctoral dissertation)*. Utah State University. Retrieved from https://core.ac.uk/download/pdf/19677055.pdf

Hunsucker, R. D., & Hargreaves, J. K. (2003). *The high-latitude ionosphere and its effects on radio propagation*. New York. Cambridge University Press.

Korsakov, A., Kozlov, V., & Toropov, A. (2020). Seasonal variations of the amplitude of the VLF radio signals and the intensity of the atmospheric electric field in Cryolithozone conditions. *IOP Conference Series: Materials Science and Engineering*, *753*, 042093. https://doi.org/10.1088/1757-899X/753/4/042093

Laskar, F. I., Chau, J. L., Stober, G., Hoffmann, P., Hall, C. M., & Tsutsumi, M. (2016). Quasi-biennial oscillation modulation of the middle- and high-latitude mesospheric semidiurnal tides during August–September. *Journal of Geophysical Research: Space Physics*, *121*, 4869–4879. https://doi.org/10.1002/2015JA022065

Livesey, N., Read, W., Wagner, P., Froidevaux, L., Santee, M., Schwartz, M., et al. (2020). *Version 5.0x level 2 and 3 data quality and description document, version 5.0-1.0a*. Pasadena, CA. Jet Propulsion Laboratory. Retrieved from https://mls.jpl.nasa.gov/data/v5-0_data_quality_document.pdf

Lübken, F. -J. (1999). Thermal structure of the Arctic summer mesosphere. *Journal of Geophysical Research*, *104*(D8), 9135–9149. https://doi.org/10.1029/1999JD900076

Macotela, E. L., Clilverd, M., Manninen, J., Moffat-Griffin, T., Newnham, D. A., Raita, T., & Rodger, C. J. (2019). D-region high-latitude forcing factors. *Journal of Geophysical Research: Space Physics*, *124*, 765–781. https://doi.org/10.1029/2018JA026049

Macotela, E. L., Clilverd, M. A., Manninen, J., Thomson, N. R., Newnham, D. A., & Raita, T. (2019). The effect of ozone shadowing on the D region ionosphere during sunrise. *Journal of Geophysical Research: Space Physics*, *124*, 3729–3742. https://doi.org/10.1029/2018JA026415

Macotela, E. L., Raulin, J. -P., Manninen, J., Correia, E., Turunen, T., & Magalhães, A. (2017). Lower ionosphere sensitivity to solar X-ray flares over a complete solar cycle evaluated from VLF signal measurements. *Journal of Geophysical Research: Space Physics*, *122*, 12370–12377. https://doi.org/10.1002/2017JA024493

McRae, W. M., & Thomson, N. R. (2000). VLF phase and amplitude: Daytime ionospheric parameters. *Journal of Atmospheric and Solar-Terrestrial Physics*, *62*(7), 609–618. https://doi.org/10.1016/S1364-6826(00)00027-4

Neal, J. J., Rodger, C. J., Clilverd, M. A., Thomson, N. R., Raita, T., & Ulich, T. (2015). Long-term determination of energetic electron precipitation into the atmosphere from AARDDVARK subionospheric VLF observations. *Journal of Geophysical Research: Space Physics*, *120*, 2194–2211. https://doi.org/10.1002/2014JA020689

Nicolet, M., & Aikin, A. C. (1960). The formation of the D region of the ionosphere. *Journal of Geophysical Research*, *65*(5), 1469–1483. https://doi.org/10.1029/JZ065i005p01469

Pal, S., & Hobara, Y. (2016). Mid-latitude atmosphere and ionosphere connection as revealed by very low frequency signals. *Journal of Atmospheric and Solar-Terrestrial Physics*, *138–139*, 227–232. https://doi.org/10.1016/j.jastp.2015.12.008

Pancheva, D., & Mukhtarov, P. (1996). Modelling of the electron density height profiles in the mid-latitude ionospheric D-region. *Annali di Geofisica*, *39*(4). https://doi.org/10.4401/ag-4021

Pedatella, N. M., Liu, H. -L., Conte, J. F., Chau, J. L., Hall, C., Jacobi, C., et al. (2021). Migrating semidiurnal tide during the September equinox transition in the Northern Hemisphere. *Journal of Geophysical Research: Atmospheres*, *126*, e2020JD033822. https://doi.org/10.1029/2020JD033822

Renkwitz, T., Tsutsumi, M., Laskar, F. I., Chau, J. L., & Latteck, R. (2018). On the role of anisotropic MF/HF scattering in mesospheric wind estimation. *Earth Planets and Space*, *70*, 158. https://doi.org/10.1186/s40623-018-0927-0

Sandford, D. J., Muller, H. G., & Mitchell, N. J. (2006). Observations of lunar tides in the mesosphere and lower thermosphere at Arctic and middle latitudes. *Atmospheric Chemistry and Physics*, *6*, 4117–4127. https://doi.org/10.5194/acp-6-4117-2006

Shepherd, M. G., Evans, W. F. J., Hernandez, G., Offermann, D., & Takahashi, H. (2004). Global variability of mesospheric temperature: Mean temperature field. *Journal of Geophysical Research: Atmospheres*, *109*, D24117. https://doi.org/10.1029/2004JD005054

Silber, I., Price, C., Rodger, C. J., & Haldoupis, C. (2013). Links between mesopause temperatures and ground-based VLF narrowband radio signals. *Journal of Geophysical Research: Atmospheres*, *118*, 4244–4255. https://doi.org/10.1002/jgrd.50379

Singer, W., Bremer, J., Hocking, W. K., Weiss, J., Latteck, R., & Zechal, M. (2003). Temperature and wind tides around the summer mesopause at middle and Arctic latitudes. *Advances in Space Research*, *31*(9), 2055–2060. https://doi.org/10.1016/S0273-1177(03)00228-X

Singer, W., Latteck, R., & Holdsworth, D. A. (2008). A new narrow beam Doppler radar at 3 MHz for studies of the high-latitude middle atmosphere. *Advances in Space Research*, *41*, 1488–1494. https://doi.org/10.1016/j.asr.2007.10.006

Smith, A. K. (2012). Global dynamics of the MLT. *Surveys in Geophysics*, *33*, 1177–1230. https://doi.org/10.1007/s10712-012-9196-9

Stening, R. J., Schlapp, D. M., & Vincent, R. A. (1997). Lunar tides in the mesosphere over Christmas Island (2°N, 203°E). *Journal of Geophysical Research*, *102*(D22), 26239–26245. https://doi.org/10.1029/97JD00898

Thomson, N. R., Clilverd, M. A., & Rodger, C. J. (2017). Midlatitude ionospheric D region: Height, sharpness and solar zenith angle. *Journal of Geophysical Research: Space Physics*, *122*, 8933–8946. https://doi.org/10.1002/2017JA024455

Wait, J. R., & Spies, K. P. (1964). *Characteristics of the Earth-ionosphere waveguide for VLF radio waves. Volume NBS technical note 300*. NIST Research Library.

Waters, J. W., Froidevaux, L., Harwood, R. S., Jarnot, R. F., Pickett, H. M., Read, W. G., et al. (2006). The Earth observing system microwave limb sounder (EOS MLS) on the aura satellite. *IEEE Transactions on Geoscience and Remote Sensing*, *44*(5), 1075–1092. https://doi.org/10.1109/TGRS.2006.873771

Watt, A. D. (1967). *VLF radio engineering*. Pergamon Press.